





RESEARCH ARTICLE | MARCH 30 2023

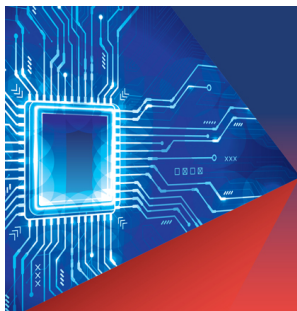
## Optimal allocation and energy management of a wind–hydrogen generation system equipped with the speed regulating differential mechanism

Wen-liang Yin  ; Lin Liu   ; Yue Wang; Zi-wei Wang; Jun-hui Li 



*J. Renewable Sustainable Energy* 15, 023302 (2023)

<https://doi.org/10.1063/5.0134039>



**Journal of Renewable and Sustainable Energy**

**Special Topic:**  
**Smart Hybrid Renewable Energy Harvesting Systems: An IoT-Based Approach**

Guest Editors: Abdu Saif, Manoj Kumar and Sachin Kumar Gupta

**Submit Today!**

# Optimal allocation and energy management of a wind–hydrogen generation system equipped with the speed regulating differential mechanism

Cite as: J. Renewable Sustainable Energy **15**, 023302 (2023); doi: 10.1063/5.0134039

Submitted: 8 November 2022 · Accepted: 14 March 2023 ·

Published Online: 30 March 2023



View Online



Export Citation



CrossMark

Wen-liang Yin,<sup>1,2,a)</sup>  Lin Liu,<sup>3,b)</sup>  Yue Wang,<sup>2,c)</sup>  Zi-wei Wang,<sup>2,d)</sup>  and Jun-hui Li<sup>1,e)</sup> 

## AFFILIATIONS

<sup>1</sup>Key Laboratory of Modern Power Simulation and Control & Renewable Energy Technology, Ministry of Education, Northeast Electric Power University, Jilin 132012, China

<sup>2</sup>School of Electrical and Electronic Engineering, Shandong University of Technology, Zibo 255000, China

<sup>3</sup>School of Electrical and Data Engineering, University of Technology Sydney, Sydney, NSW 2007, Australia

<sup>a)</sup>Electronic mail: [yinwenliang@sdut.edu.cn](mailto:yinwenliang@sdut.edu.cn). Tel.: +8615011006609

<sup>b)</sup>Author to whom correspondence should be addressed: [Lin.Liu-1@uts.edu.au](mailto:Lin.Liu-1@uts.edu.au). Tel.: +61416699028

<sup>c)</sup>Electronic mail: [NYDL\\_vy@163.com](mailto:NYDL_vy@163.com)

<sup>d)</sup>Electronic mail: [20404010482@stumail.sdut.edu.cn](mailto:20404010482@stumail.sdut.edu.cn)

<sup>e)</sup>Electronic mail: [lijunhui@neepu.edu.cn](mailto:lijunhui@neepu.edu.cn)

## ABSTRACT

The hybrid drive wind turbine (WT) can be friendly connected to the power grid by using a speed regulating differential mechanism (SRDM) instead of partially or fully rated converters, which has been considered as a promising solution for the stable consumption of large-scale wind power generation. To further improve the on-grid performance of hybrid drive WTs, this paper develops a multi-source power generation scheme, in which a hydrogen storage system (HSS) is integrated for mitigating the wind power generation intermitencies. The overall architecture and kinematic principles of the proposed wind–hydrogen generation system, called SRDM-based WT with HSS, are first analyzed. Then, the graphical descriptions of mathematical models are finalized via the Energetic Macroscopic Representation method, by which the physical characteristics and energy flow relationships are revealed. To ensure the economical and stable operation of the proposed wind–hydrogen scheme, an effective optimal allocation framework, considering the uncertainties from wind power output and load demand, is presented to HSS, targeting the maximum annual revenue. The effects of several key HSS parameters on the capacity allocation results are also investigated. Moreover, aiming at the different system working modes, an energy management approach is synthesized to achieve the interaction analysis and power supervision between energy sources and storage elements. Finally, experimental and simulation case studies are demonstrated. Results illustrate the effectiveness of the proposed approaches and the optimal performance for uninterrupted on-grid operation of the proposed wind–hydrogen energy system.

Published under an exclusive license by AIP Publishing. <https://doi.org/10.1063/5.0134039>

## I. INTRODUCTION

The rising in climate change and awareness of renewable energy transition has contributed to the continuous growth of wind power penetration levels around the world.<sup>1</sup> As released by the Global Wind Energy Council, over 355 GW of new wind farm capacity will be added between 2020 and 2024. It means nearly 71 GW of new installations each year till 2024.<sup>2</sup> Despite the favorable development feasibility and appreciable commercial competitiveness of wind power generation, there are still challenges in nowadays wind energy industry.

The primary challenge is that most of the existing wind farms can hardly provide electrical power with an instant match to the electricity demand as wind volatility and intermittency natures.<sup>3,4</sup> Additionally, the problems such as increasing the frequency modulation and peak shaving difficulty, damaging the grid power quality, and depraving the operational stability of the power system can also be aroused with high shares of wind power generation. As a result, grid operators have to enable wind curtailment plans, which undoubtedly hinders the friendly on-grid wind power consumptions.<sup>3–5</sup> On the other hand, wind turbines (WTs) with the working mode of variable-speed

constant-frequency (VSCF) are widely adopted for most grid-connected wind farms to optimize the energy capture efficiency and reduce the adverse grid-effects caused by wind power fluctuations.<sup>5,6</sup> To date, the dedicated double-fed induction generators (DFIGs) and direct drive synchronous generators (SGs), equipped with partly or fully rated converters, are usually required for VSCF WT's to decouple the variable wind wheel speed and the stable grid frequency.<sup>6</sup> These schemes may result in some disadvantages, such as the unreliable power system stability because of the weak low voltage ride through (LVRT) capability,<sup>7,8</sup> the decline in power quality owing to the harmonic pollutants excited by the rectifier-inverter links,<sup>9,10</sup> the huge energy dissipation, and the expensive cost.<sup>11</sup>

In recent years, speed regulating differential mechanisms (SRDMs), mainly consisting of special mechanical gear sets and hydraulic or electrical actuators, have been widely used as speed regulators at the front-end of synchronous generators (SGs), to effectively handle the above-mentioned shortcomings in VSCF WT's. Within these schemes, SG can produce grid-frequency electricity by SRDMs instead of power-consuming converters.<sup>12–24</sup> Researchers have also done substantial works about the grid-friendly front-end speed regulating WT's concerning (i) the kinematic principles and scheme design methods,<sup>12,13</sup> (ii) the power splitting behaviors and the overall transmission efficiency,<sup>14,15</sup> (iii) the adaptive or robust control approaches for guaranteeing the desired SRDM speed adjustment ability,<sup>16–19</sup> and for realizing the maximal power point tracking,<sup>20,21</sup> and (iv) the feasibility verifications of the transmission schemes with simulations and experiments.<sup>17–19,22–24</sup> The new-type WT's were also proved to have crucial advantages in elevating energy efficiency, promoting on-grid performance, saving the total costs, and relieving the challenges of large-scale wind power utilization.

Aiming at these superiorities, coupled with a planetary gear train (PGT) and a controllable permanent magnet synchronous motor (PMSM), the authors developed a novel front-end speed regulating WT called SRDM-based WT, which can be directly connected to the power grid for constant-frequency electricity production. The kinematic and dynamic characteristics and the improved PMSM speed control approaches were investigated, while the availability and ascendancy were also demonstrated.<sup>15,18,19,24</sup> However, despite the merits in frequency stability and power quality of the proposed SRDM-based WT, unstable wind power injection is still a critical challenge for the power system. That is, substantial efforts are still required to further promote the on-grid transient/steady operating performance of SRDM-based WT and therefore enhance the reliability, resilience, and flexibility of the power grid.

So far, consuming excess electricity for energy storage of resource production is considered a suitable measure to relieve the problems from large-scale and high-penetration of wind power injection.<sup>25,26</sup> Among various energy storage forms, electrolysis-based hydrogen storage systems (HSSs) have been paid more and more attention due to the features of long-term storage and almost no environmental pollutants.<sup>27–29</sup> By integrating supercapacitors, the undesired slow dynamic behaviors of HSS can be facilitated.<sup>30–32</sup> The advantages for installing HSS into WT's are mainly manifested in that (i) the grid performance is improved by capacity firming and resource diversification, (ii) the complexity of peak shaving, fluctuation of power injection as well as the adverse effects on frequency and voltage stability of power grid can all be relieved, and (iii) the CO<sub>2</sub> emissions from transportation fuel and chemical hydrogen production are reduced.<sup>27–32</sup>

To promote the on-grid performance of VSCF WT's, in our previous publications,<sup>33,34</sup> an architecture of the SRDM-based WT with HSS was developed and its numerical modeling and power flow analysis methods were presented. This paper aims to synthesize optimal allocation and energy management of the developed wind-hydrogen system. The contributions are manifested in that (i) the graphical descriptions of system models are realized through the Energetic Macroscopic Representation (EMR) method to reveal the energy flow situations; (ii) the optimal allocation of HSS is finalized, considering the uncertainties of wind power output and load demand, by which the system operation economy can be guaranteed; and (iii) the advanced energy management strategies are investigated to ensure the smooth and stable power supervision between energy sources and storage elements.

The remainder of this paper is arranged below. Section II introduces the structure and mathematical models of the SRDM-based WT with HSS. In Sec. III, the optimal allocation and energy management strategies are investigated. In Sec. IV, case studies for capacity allocation are conducted under diverse wind utilization levels, various transmission efficiencies, and investment costs of HSS. In Sec. V, a dedicated simulation platform of 3 MW SRDM-based WT with HSS is developed and then validated through physical experiments. Furthermore, the improved on-grid performance of the presented wind-hydrogen energy system is clearly verified with normal and faults operating conditions. Conclusions with discussions are illustrated in Sec. VI.

## II. SYSTEM DESCRIPTIONS AND MATHEMATICAL MODELS

### A. Architecture of the proposed SRDM-based WT with HSS

The proposed hybrid power production unit consists of a wind power generation system and an energy storage system, in which the former, namely, SRDM-based WT, contains wind wheel, differential gearbox, SRDM, and SG, while the latter, namely, HSS, is made up of electrolyzer, proton exchange membrane fuel cell (PEMFC), supercapacitor, gas compressor, and storage tank, as presented in Fig. 1.

As seen, the SRDM delivers energy from both wind wheel and PMSM and then transfers the compound mechanical energy to SG for generating constant-frequency electrical power to the grid. HSS is connected to a common DC bus to mitigate the wind energy abandonment and support the load demand. Specifically, when the WT output electricity is excessive, the remaining power can be consumed by electrolyzer units for hydrogen production. Once the load demand is difficult to meet, PEMFC would perform as a power source and quickly compensate for the power deviation. Meanwhile, the supercapacitor is employed to preclude the insufficient dynamic response speed of HSS.

### B. Speed regulating principles of SRDM

In the proposed WT, a special speed regulating device called SRDM is installed in the high-speed shaft of step-up gearbox, by which the SG rotational speed can be adjusted to constant. PGT, as a key component of SRDM, is used to compound the speeds and powers from two independent driving links. Based on the structural optimization results,<sup>15</sup> the planet carrier is desired to be connected to the step-up gearbox to transmit the dominating input from the wind wheel. The ring gear is linked with a PMSM to arrange the speed regulating



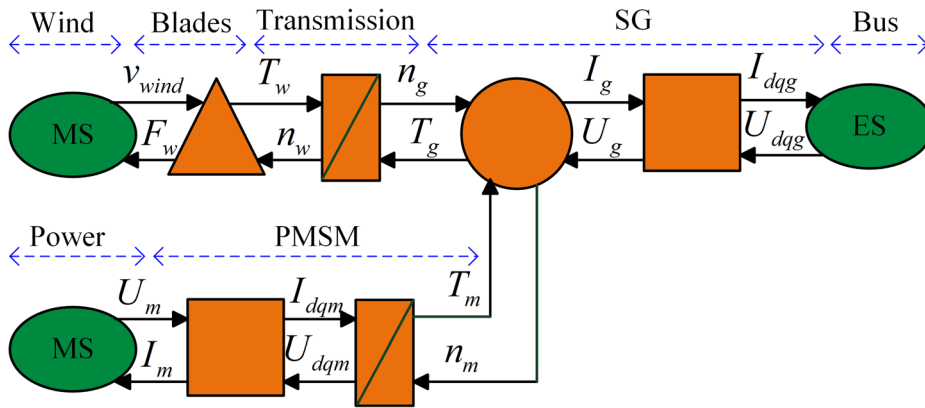


FIG. 3. EMR model of SRDM-based WT.

voltages of SG and PMSM in the three-phase stationary coordinate system.

### D. Mathematical models of HSS

#### 1. Electrolyzer

As given in the HSS operating principles, electrolyzer units consume the remaining electricity of SG, by which water is electrolyzed, then hydrogen and oxygen are obtained in cathode and anode, respectively. The voltage of a single electrolytic cell at a given temperature can be obtained through<sup>31,32</sup>

$$U_{el} = U_{rev} + \frac{a_1 + a_2 T_{el}}{A_{el}} I_{el} + (b_1 + b_2 T_{el} + b_3 T_{el}^2) \lg \left( \frac{c_1 + c_2/T_{el} + c_3/T_{el}^2}{A_{el}} I_{el} + 1 \right). \quad (7)$$

Then, according to Faraday's law, when cooperating  $N_{el}$  electrolytic cells in series, the hydrogen evolution rate ( $N_{H_2}$ ) of electrolyzer units can be expressed as follows:

$$\begin{cases} N_{H_2} = \eta(T_{el}, I_{el}) \frac{N_{el}}{2F} I_{el}, \\ \eta(T_{el}, I_{el}) = d_1 \exp \left[ \frac{d_2 + d_3 T_{el} + d_4 T_{el}^2}{(T_{el}/A_{el})} + \frac{d_5 + d_6 T_{el} + d_7 T_{el}^2}{(I_{el}/A_{el})^2} \right]. \end{cases} \quad (8)$$

The total amount of hydrogen production ( $M_{H_2}$ ) is

$$M_{H_2} = \int_{t_1}^{t_2} N_{H_2} dt. \quad (9)$$

In (7)–(9),  $U_{rev}$  is the reversible voltage of the electrolytic cell,  $N_{el}$  is the electrolytic cell number, and  $U_{A_{el}}$  is the voltage by combining  $N_{el}$  electrolytic cells.  $I_{eb}$ ,  $T_{eb}$ , and  $A_{el}$  are the inductor current, electrode area, and working temperature of the electrolyzer.  $\eta(T_{el}, I_{el})$  and  $F$  are the Faraday efficiency and constant.  $t_1$  and  $t_2$  are the start and end times for hydrogen production.  $a_1$  and  $a_2$  are the Ohmic parameters of electrolytes.  $b_1$ ,  $b_2$ ,  $b_3$ ,  $c_1$ ,  $c_2$ , and  $c_3$  are all the electrode overvoltage parameters.  $d_j$  ( $j = 1, 2, \dots, 7$ ) are empirical parameters. All the electrolyzer parameters are listed in Table I of Appendix A.<sup>31,32</sup>

#### 2. Proton exchange membrane fuel cell

The output voltage of PEMFC units ( $U_{A_{fc}}$ ) is calculated as

$$U_{A_{fc}} = N_{fc} U_{fc}, \quad (10)$$

where  $N_{fc}$  is the number PEMFCs, and  $U_{fc}$  is the output voltage of a single fuel cell which is calculated as<sup>32</sup>

$$U_{fc} = E_n^0 + \frac{QT_{fc}}{2F} \ln \left( \frac{p_{H_2} \cdot p_{O_2}^{0.5}}{p_{H_2O}} \right) - \frac{QT_{fc}}{\alpha nF} \ln \left( \frac{I_{fc}}{i_{ex0}} \right) - \frac{QT_{fc}}{nF} \ln \left( 1 - \frac{I_{fc}}{I_{lim}} \right) - I_{fc} R_{fc}, \quad (11)$$

where  $p_{H_2}$ ,  $p_{O_2}$ ,  $p_{H_2O}$  are the effective partial pressures of  $H_2$ ,  $O_2$ , and  $H_2O$ .  $I_{fc}$ ,  $I_{ex0}$ ,  $I_{lim}$ ,  $T_{fc}$ , and  $R_{fc}$  are the current, exchanged limit currents, temperature, and resistance of PEMFC.  $Q$  is the gas constant.  $\alpha$  and  $n$  are both constant parameters.

The mathematical models of the storage tank, air compressor, and supercapacitor introduced in Refs. 31 and 32 are utilized. Finally, the EMR model of the proposed SRDM-based WT with HSS can be established in Fig. 4, where the subscripts *el*, *fc*, *WT*, *sc*, *grid*, *imp*,  $H_2$ , and  $O_2$  represent the electrolyzer, PEMFC, WT, supercapacitor, power grid, high-voltage side of DC/DC converter, hydrogen, and oxygen, respectively.  $U_{DC}$  is the modulation voltage in the low-voltage side of the DC/DC converter, and  $I_{Le}$  the inductance current.

### III. OPTIMAL ALLOCATION AND ENERGY MANAGEMENT STRATEGIES

#### A. Optimal allocation of the SRDM-based WT with HSS

Concerns over the relatively high technical and investment costs of HSS have contributed to the following investigations of the capacity allocation optimization for the proposed wind–hydrogen hybrid energy system. In this study, the goal is to find the optimal allocations of key parts in SRDM-based WT with HSS by means of maximizing the annual project profits while maintaining the high-level wind energy utilization rate. The stochastic variables from the wind and load demand as well as the constraints for the safe operation of each sub-system are considered. The optimization parameters involve the capacities of the electrolyzer, PEMFC, air compressor, hydrogen storage tank, and supercapacitor, marked via  $C_{eb}$ ,  $C_{fc}$ ,  $C_{comp}$ ,  $C_D$ , and  $C_{sc}$  respectively.

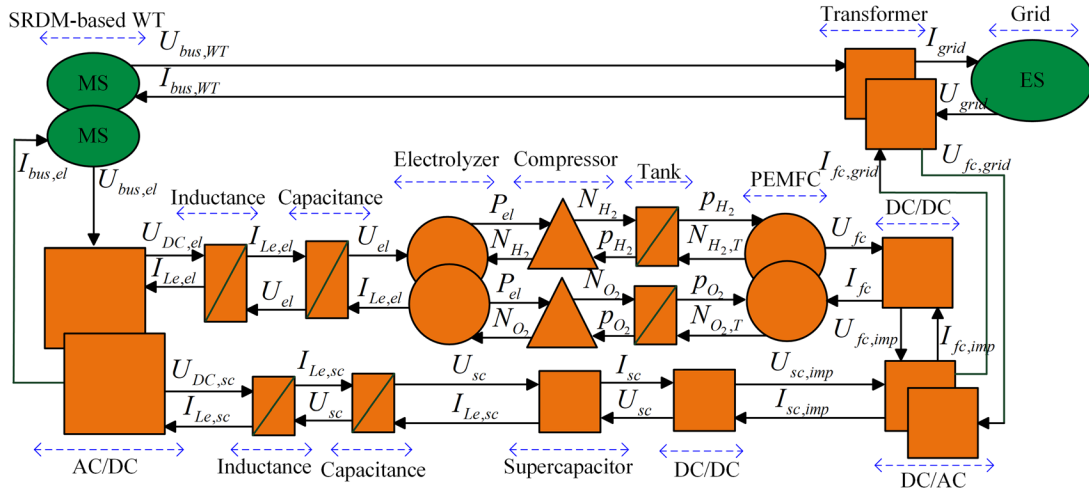


FIG. 4. EMR model of the proposed SRDM-based WT with HSS.

1. Formulation of the objective function

The total cost of SRDM-based WT with HSS consists of three items, namely, the investment cost ( $M_1$ ), operation and maintenance cost ( $M_2$ ), and additional operation cost ( $M_3$ ).

$$M_{total} = M_1 + M_2 + M_3. \quad (12)$$

The investment involves all the six components of SRDM-based WT with HSS, including the WT, electrolyzer, PEMFC, air compressor, hydrogen storage tank, and supercapacitor. In order to convert the initial payments into annual terms, the capital factors ( $A_k$ ) are defined with

$$A_k = \frac{d_k(1 + d_k)^{N_k}}{(1 + d_k)^{N_k+1} - 1} \quad k = WT, el, fc, com, t, sc, \quad (13)$$

where  $d_k$  are the discount rates, and  $N_k$  the equipment lifespans.

Then, the annual investment cost can be evaluated by

$$M_1 = \sum_k A_k \bar{M}_{1k} C_k, \quad k = WT, el, fc, com, t, sc. \quad (14)$$

Since the operation and maintenance costs per unit are fixed,  $M_2$  can be calculated via

$$M_2 = \sum_k \bar{M}_{2k} C_k, \quad k = WT, el, fc, com, t, sc. \quad (15)$$

In Eqs. (17) and (18),  $\bar{M}_{1k}$  and  $\bar{M}_{2k}$  donate the investment cost and the fixed operation/maintenance cost per unit.

The additional operation cost contains two parts, the wind curtailment penalty cost ( $M_{pen}$ ) which exists once the HSS reaches its maximum capacity and the energy purchase cost ( $M_{pur}$ ) for maintaining the continuous operation of HSS. The transmission cost for electricity and hydrogen is not considered since they will be sold directly to the local grid and chemical companies. Thus,  $M_3$  can be evaluated through<sup>37</sup>

$$M_3 = M_{pen} + M_{pur} = \sum_{t=1}^T \bar{M}_{pen} P_{pen,t} + \sum_{t=1}^T \bar{M}_{pur} P_{pur,t}, \quad (16)$$

where  $\bar{M}_{pen}$  and  $\bar{M}_{pur}$  are the average values of  $M_{pen}$  and  $M_{pur}$  per unit.  $P_{pen,t}$  and  $P_{pur,t}$  are the wind curtailment power and the power supplied by the substation at time  $t$ .

It should be noted that the wind curtailment penalty cost exists when the HSS reaches its maximum capacity and is not able to consume all power gaps between WT and load demand.

The total project benefits can be evaluated with

$$B_{total} = B_1 + B_2 + B_3. \quad (17)$$

$B_1$  is the benefit coming from electricity sales and given as

$$B_1 = u_{ws} E_{ws} + u_{fc} E_{fc} \quad (18)$$

with

$$\begin{cases} E_{ws} = \sum_{t=1}^T P_{ws,t}, \\ E_{fc} = \sum_{t=1}^T P_{fc,t}, \end{cases} \quad (19)$$

where  $u_{ws}$  and  $u_{fc}$  represent the on-grid electricity tariffs from WT and PEMFC.  $P_{ws,t}$  and  $P_{fc,t}$  are the average on-grid powers transmitted by WT and PEMFC at time  $t$ .

$B_2$  is the benefit from hydrogen sales and calculated as

$$B_2 = u_{hs} E_{hs} = u_{hs} \sum_{t=1}^T P_{hs,t}, \quad (20)$$

where  $u_{hs}$  is the average annual hydrogen price, and  $P_{hs,t}$  is the release rate of hydrogen tank at time  $t$ .

$B_3$  is the environmental profit that benefited from the government subsidies for wind energy ( $B_{gov}$ ) as well as the cost reduction due to the hydrogen production ( $B_{cr}$ ).

$$B_3 = B_{gov} + B_{cr} \quad (21)$$

with

$$B_{cr} = C_{fh} + C_{ecr}, \quad (22)$$

where  $C_{fh}$  is the electricity cost for hydrogen production by coal,  $C_{ecr}$  is the environmental cost for electricity generation by coal, and

$$C_{ecr} = \sum_{h=1}^H (\Delta m_h \lambda_h + \Delta m_h \mu_h), \quad (23)$$

where  $H$  is the pollutant category, and  $\Delta m_h$  is the reduced amount of the  $h$ th pollutant owing to WT.  $\lambda_h$  and  $\mu_h$  are the environmental value and penalty coefficient of the  $h$ th pollutant.

Then, the optimal objective function can be expressed via

$$\max f(C_{el}, C_{fc}, C_{com}, C_t, C_{sc}) = B_{total} - M_{total}. \quad (24)$$

## 2. Formulation of the constraints

*a. Balance equation of WT power.* The electrical power generated by WT should be transmitted to the grid and the electrolyzer; otherwise, it will be wasted. Also,

$$P_{WT,t} = P_{ws,t} + P_{el,t} + P_{pen,t}, \quad (25)$$

where  $P_{el,t}$  is the power transmitted to the electrolyzer at time  $t$ .

*b. Balance equations of HSS power flow.* The power absorbed from WT and purchased from the grid should be both employed to produce hydrogen. Meanwhile, the hydrogen is for sale and can be transmitted to PEMFC for electricity generation.

$$\begin{cases} P_{H_2,t} = (P_{el,t} + P_{pur,t} + \gamma P_{sc,t}) \eta_{el} \eta_{com}, \\ P_{H_2,t} = P_{hs,t} + P_{fc,t} / \eta_{fc}, \end{cases} \quad (26)$$

where  $P_{H_2,t}$  and  $P_{fc,t}$  are hydrogen storage power and PEMFC power at time  $t$ .  $\eta_{eb}$ ,  $\eta_{com}$ , and  $\eta_{fc}$  are the working efficiencies of the electrolyzer, compressor, and PEMFC, respectively.  $P_{sc,t}$  is the power of supercapacitor at time  $t$ . In the working mode 1,  $\gamma = 1$  holds, while in mode 3,  $\gamma = -1$  holds.

*c. Operating power constraints.* The generation capacity should constrain the operating powers of each component in SRDM-based WT with HSS. Namely,

$$\begin{cases} 0 \leq P_{ws,t} \leq P_{rated}, \\ 0 \leq P_{el,t} \leq C_{el}, \\ 0 \leq P_{fc,t} / \eta_{fc} \leq C_{fc}, \\ 0 \leq P_{sc,t} \leq C_{sc}, \\ 0 \leq P_{pen,t} \leq P_{ws,t}, \\ 0 \leq P_{hs,t} \leq P_{H_2,t}, \end{cases} \quad (27)$$

where  $P_{rated}$  is the rated power of WT.

*d. On-grid power fluctuation constraint.* It is desired that the on-grid power provided by the SRDM-based WT with HSS should fluctuate within the allowable range to guarantee the safe and stable operation of the grid.

$$|(P_{ws,t} + P_{fc,t} + \zeta P_{sc,t}) - (P_{ws,t-1} + P_{fc,t-1} + \zeta P_{sc,t-1})| \leq 0.1 P_{rated}. \quad (28)$$

*e. Optimal operating power constraint.* To ensure the economy and stability of HSS, the electrolyzer should operate in an optimized status.

$$P_{el,min} \leq P_{el,t} + P_{pur,t} + \gamma P_{sc,t} \leq P_{el,max}. \quad (29)$$

*f. Wind power utilization level constraint.* To maintain the wind power utilization level, a chance-constrained rule is employed to make sure that the wind power curtailment is smaller than  $\tau$  percent of  $P_{WT,t}$  with at least  $1 - \chi$  probability.<sup>37</sup>

$$\Pr \left[ \left( \sum_{t=1}^T P_{pen,t} - \tau \sum_{t=1}^T P_{WT,t} \right) \leq 0 \right] \geq 1 - \chi. \quad (30)$$

The detailed information for converting the chance constraint to the determined equivalent with a given confidence level can be found in Ref. 37.

## B. Coordinated control of SRDM-based WT with HSS

After finalizing the optimal allocation, an energy management approach is synthesized for the smooth operating of the presented wind-hydrogen system, in which eight diverse working modes are defined based on the running status analysis of WT, electrolyzer, supercapacitor bank, and PEMFC. Due to the space limitation, the specifically designed process of the control strategy is illustrated in Appendix B. The proposed energy management strategy and the detailed mode selection process are also depicted in Figs. 15 and 16 of Appendix B, respectively. The effective power flowing control of the HSS components can be guaranteed by the reference powers set by implementing the presented energy management approach. Then, the interaction analysis and power supervision between the energy sources and storage elements can be finalized.

Apart from the energy management strategy, for the coordinated control of equipment in SRDM-based WT, the adaptive neuro-fuzzy pitch angle control method, referenced by Petković's work,<sup>20</sup> is employed. Combined with the backstepping design method and sliding mode control theory, a backstepping sliding mode excitation control approach<sup>38</sup> is proposed by the authors team and utilized in this scheme. The brief descriptions of the control law design process are given in Appendix C. Different from the existing grid-connected VSCF WTs, SRDM-based WT aims to produce constant-frequency electric power with SRDM instead of converters. In order to make sure that the generator output power frequency is consistent with that of the power grid regardless of the parametric uncertainties and variable external disturbances, a discontinuous projection-based adaptive robust backstepping controller, combined with an improved extended state observer, is synthesized for the accurately speed control of SRDM. The structure diagram of SRDM speed control unit is designed in Fig. 17 in Appendix C. More detailed information of the SRDM speed control approach can be found in our previous publication.<sup>19</sup>

Taking advantage of the current single-loop PI control method, the control equations of DC-DC transverters that are linked with electrolyzer, supercapacitor, and PEMFC can be described as Eqs. (31), (32), and (33), respectively,

$$D_{el} = \left( K_{el_p} + \frac{K_{el_l}}{s} \right) \left( \frac{P_{el}^*}{U_{el}} - I_{el} \right), \quad (31)$$

$$D_{sc} = \left( K_{sc_p} + \frac{K_{sc_l}}{s} \right) \left( \frac{P_{sc}^*}{U_{sc}} - I_{sc} \right), \quad (32)$$

$$D_{fc} = \left( K_{fc_p} + \frac{K_{fc_l}}{s} \right) \left( \frac{P_{fc}^*}{U_{fc}} - I_{fc} \right), \quad (33)$$

where  $K_{el_p}$ ,  $K_{sc_p}$ , and  $K_{fc_p}$  are the proportional factors of the electrolyzer, supercapacitor, and PEMFC, whereas  $K_{el_l}$ ,  $K_{sc_l}$ , and  $K_{fc_l}$  are their integral factors.  $I_{el}$ ,  $I_{sc}$ ,  $I_{fc}$  and  $P_{el}^*$ ,  $P_{sc}^*$ ,  $P_{fc}^*$  represent the actual operating currents and reference powers of the electrolyzer, supercapacitor, and PEMFC, respectively.

After calculating the quotient of  $P_{el}^*$  and  $U_{el}$ , as the desired current, the electrolyzer control signal can be constructed to be the difference between the reference and actual current values. As shown in Eqs. (32) and (33), similar control schemes are also applied to the supercapacitor and PEMFC. In this case, the control strategies in equipment-level of both the SRDM-based WT and HSS are all finalized. That is, once the commands are determined by the energy management center, the control strategies in equipment-level can respond to the energy management instructions to realize the stable operation of the whole system.

#### IV. CASE STUDIES FOR OPTIMAL ALLOCATION

##### A. Parameters setting

Since the above-mentioned capacity allocation of SRDM-based WT with HSS is a nonlinear robust optimization problem, the

enhanced column-and-constraint generation algorithm, proven to have advantages in terms of strong ability to find the optimal global solution with fast speed and strong robustness, stability, and adaptability,<sup>39</sup> is utilized for solving the optimization model. The key parameters and data for capacity allocation solving are all given in Table II of Appendix A. The rated power of SRDM-based WT is 3 MW. All the data in Table II are confirmed according to the documents provided by the demonstration project located in Inner Mongolia, China.

##### B. Planning results

Taking advantage of the established objective function and constraints, the optimization model is solved with the particle swarm optimization (PSO) method through MATLAB software.

During the optimization process, four cases of different wind power utilization levels, including, case I:  $1 - \tau = 0.80$ , case II:  $1 - \tau = 0.85$ , case III:  $1 - \tau = 0.90$ , and case IV:  $1 - \tau = 0.95$ , all with  $1 - \chi = 0.8$ , are set for the planning and investigations of wind power permeability effects. Figures 5(a) and 5(c) show the capacity allocation results obtained during the whole lifespan.

As seen, along with the increase in the wind power utilization level, the capacity of HSS needs to be expanded. Compared to the results of case I, the capacities of the electrolyzer, PEMFC, air compressor, hydrogen storage tank, and supercapacitor for case II grow by 9.52%, 7.46%, 6.48%, 10.22%, and 8.38%. The HSS capacity results of cases III and IV increase by 11.34%–17.06% and 23.15%–28.85%, respectively. However, as the investment, operational, and maintenance costs of HSS are relatively high, the net profits of the project are gradually decreased with  $1 - \tau$  growth. Compared with case I,

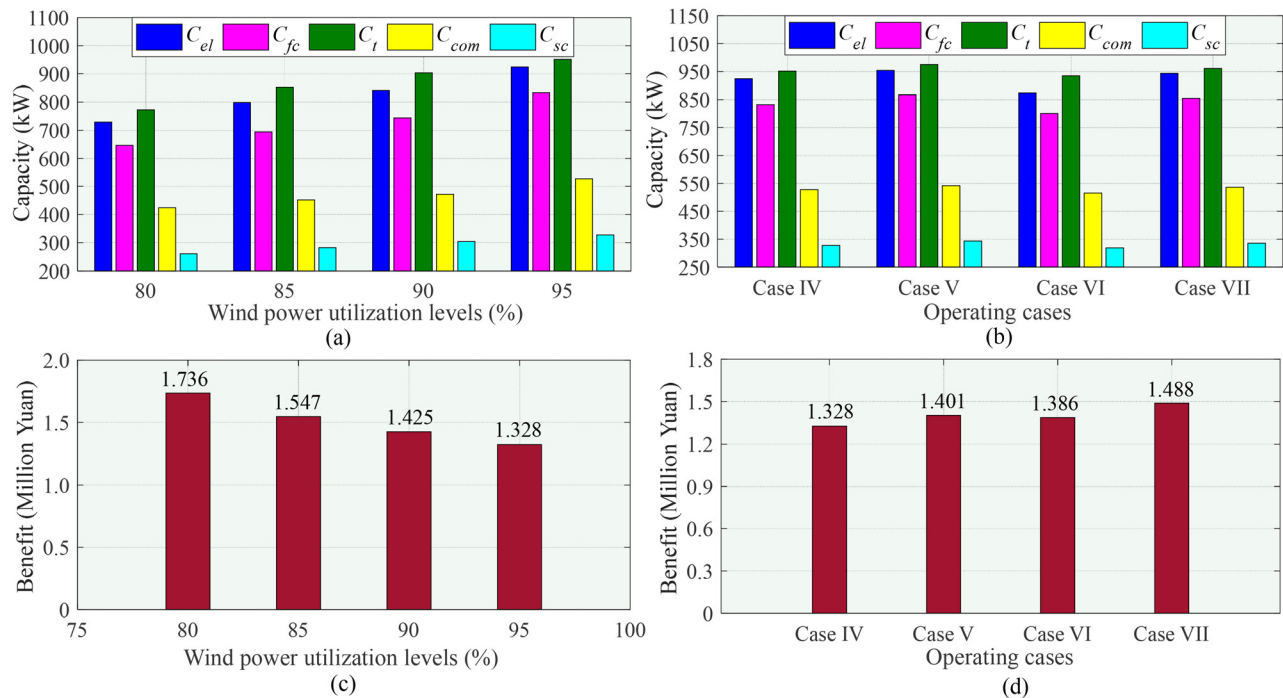


FIG. 5. Optimal results with different wind power utilization levels, investment costs, and operating efficiencies: (a) capacity results under different wind utilization levels, (b) capacity results of the defined operating cases, (c) benefit results under different wind utilization levels, and (d) benefit results of the defined operating cases.



the profits under cases II, III, and IV decrease by 0.189, 0.311, and  $0.408 \times 10^6$  Yuan.

To date, the investment cost and working efficiency of HSS are key influencing factors for the optimal capacity allocation of the wind-hydrogen hybrid energy system. In this subsection, with 95% wind power utilization level and 0.8 confidence level, case V (investment cost of HSS is decreased by 5%), case VI (working efficiencies of electrolyzer and PEMFC are promoted by 5%) as well as case VII (the investment cost is reduced by 5% and the working efficiencies are promoted by 5%) are set to investigate the corresponding influences. The optimal capacity allocation results are presented in Figs. 5(b) and 5(d).

With the development of HSS technology, the relatively high investment cost and low working efficiencies of HSS must be ameliorated. Compared to case IV, HSS capacity and project benefit, under case V, increase by 2.46%–4.82% and 5.50%, respectively. Under case VI, the HSS capacity decreases by 1.74%–5.44%, while the benefit increases by 4.37%. Under case VII, the HSS capacity and benefit increase by 1.03%–2.68% and 12.05%, respectively.

## V. PERFORMANCE VERIFICATIONS

As far as the authors know, integrating HSS to the SRDM-based WT provides a potential solution for improving not only the wind power utilization level but also the on-grid operating adaptability and stability of SRDM-based WT, compared to the existing VSCF WTs. Therefore, based on the mathematical models and optimal capacity allocation results, a dedicated Simulink platform of SRDM-based WT with HSS is developed for simulation studies of performance verifications.

### A. Experimental verification of the simulation platform

The simplified triaxial dynamics could bring modeling errors to the simulation platform. Therefore, experiments on different wind conditions are demonstrated to show the availability and accuracy of the used simulation approach. In the subsection, Simulink built-in package modules of PMSM, SG, and power grid are employed, while the Solidworks software is adapted to obtain the moments of inertia of transmission shafts. Moreover, for convincing validations, the simulation model is established by using the practical parameters of the experimental platform, of which construction and detailed working principles are outlined in Figs. 18 and 19 in Appendix D, respectively.

The normal turbulent wind models with average speeds of 5, 10, 13, and 21 m/s and 20% turbulence intensity are generated through FAST software, while the corresponding wind wheel speeds are also obtained to be the input sources for both experiments and simulations, as shown in Fig. 6. Define the working time as 100 s, the reference SG rotational speed as 300 rpm. Then, the simulation and experimental results of SRDM output speeds are recorded in Fig. 7.

As shown, the SRDM output speeds from experiments and simulations can all be stably maintained at around 300 rpm despite the different wind speed inputs. Compared to the ideal value, the maximum and the average steady-state speed errors in experiments are less than 2.40% (7.20 rpm) and 1.66% (4.99 rpm), while the errors in simulations are all within 1.34% (4.01 rpm) and 1.02% (3.06 rpm), respectively. The results show the acceptable availability and accuracy of the built simulation platform, which commendably supports the following works about the operating performance verifications.

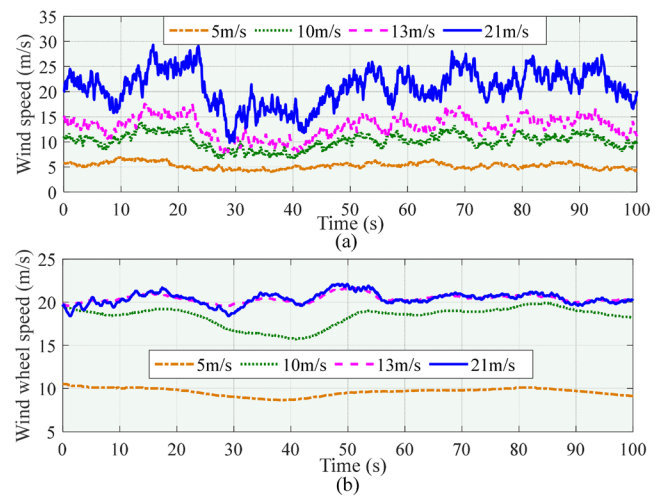


FIG. 6. Profiles of wind speeds and wind wheel speeds: (a) wind speeds and (b) wind wheel speeds.

### B. Operating performance under normal conditions

After the experimental verifications of the simulation method, a dedicated simulation platform of a 3 MW SRDM-based WT with HSS is developed based on the derived mathematical expressions as well as the optimal allocation results. The key parameters of the 3 MW SRDM-based WT can be found in Ref. 15.

According to the international standard IEC-61400-1, four typical wind models are generated as system inputs for the following simulations. They are case (1): normal turbulent model with 10 m/s average speed and 20% turbulence intensity, case (2): extreme turbulent model with 13 m/s speed, 40% turbulence, case (3): extreme operating gusts with 10 m/s initial speed, 6.82 m/s gust variation amplitude, and case (4): extreme coherent gusts with 10 m/s initial speed, 14.88 m/s gust amplitude,  $-72^\circ$  change in direction.

In order to show the improved performance in terms of speed regulation and transmission efficiency of the developed SRDM-based WT, a special working mode is simulated, in which all the SG output power is transmitted to HSS for hydrogen production. After the 100 s simulation period, the operation indicators of SRDM output speeds that reflect directly to the frequency of output electricity, powers delivered by SG and PMSM, as well as the comparative hydrogen production capacities between SRDM- and DFIG-based WTs are all recorded in Figs. 8–11. The data analysis of Figs. 8–11 is given as follows. (i) SRDM can regulate the SG rotational speeds to the range of [1480, 1520] whatever the wind input conditions are. The maximum steady-state errors are all less than 1.27%, whereas the average steady-state errors are all within 0.38%, which can perfectly meet the guidelines of the National Standard GB/T15945–2008 of China.<sup>40</sup> (ii) The maximum power consumption required by PMSM is less than 483.2 kW, which accounts for only 17.73% of the SG power and indicates the advancement of the SRDM-based WT in energy transmission efficiency. (iii) Compared to the existing DFIG-based WT, SRDM-based WT can generate more hydrogen in amount, by around 7.51%, 5.84%, 7.19%, and 6.15% under the four cases of wind inputs, respectively.

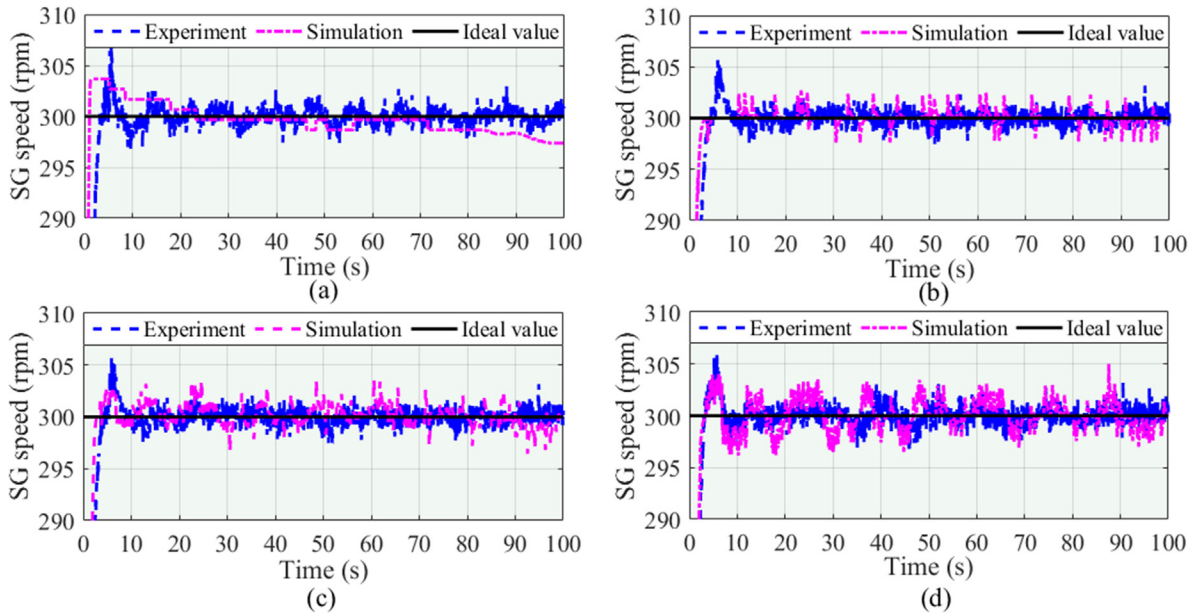


FIG. 7. Comparative results of SRDM output speeds under different wind inputs: (a) 5, (b) 10, (c) 13, and (d) 21 m/s.

The grid-connected operating performance is also verified under the normal turbulent wind speed model. After giving the load demand, the power balance of SRDM-based WT with HSS is studied, as shown in Fig. 12. It is obvious that the electrolyzer and PEMFC have satisfactory dynamic characteristics and can track the reference power values quickly, stably, and accurately. Meanwhile, the grid-connected power

can also well-meet the load demand. As seen in Fig. 12(d), the maximum and average deviations between the on-grid power and load demand are remarkably reduced into around 4.15% and 11.69% of rated power (3 MW), respectively. Moreover, according to Figs. 12(a) and 12(d), HSS, working as a power balancer, can efficiently suppress the instant fluctuations in the on-grid power of the presented system.

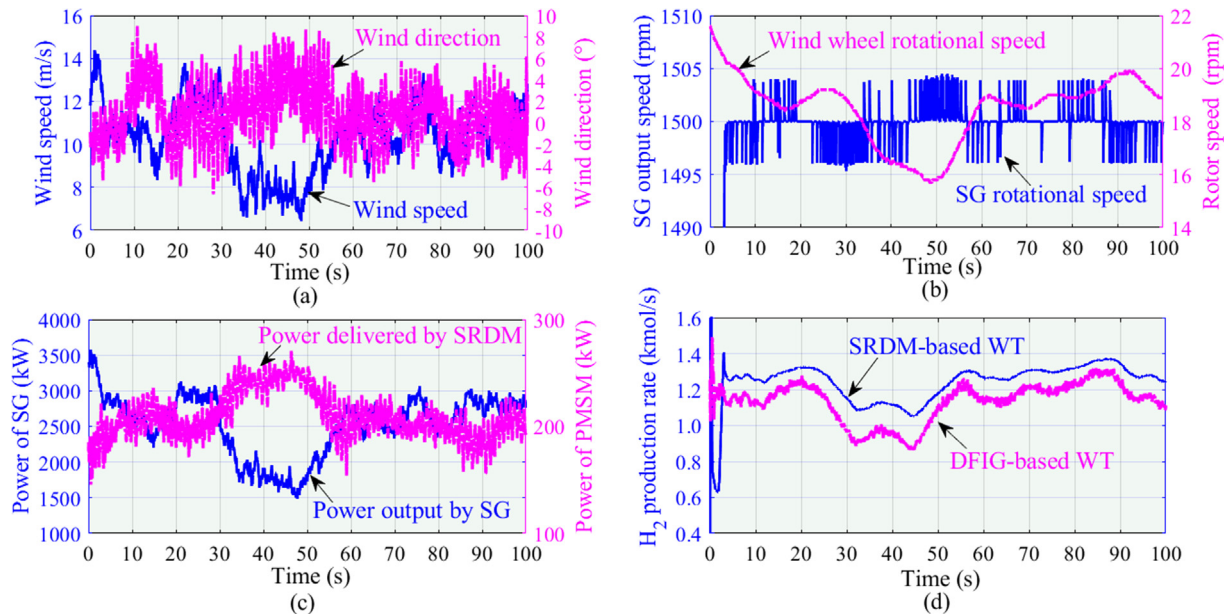


FIG. 8. Operating performance results of the proposed system under case (1): (a) wind wheel input, (b) speeds of wind wheel and SG, (c) power delivered by SG and SRDM, and (d) hydrogen production rates with SRDM- and DFIG-based WTs.

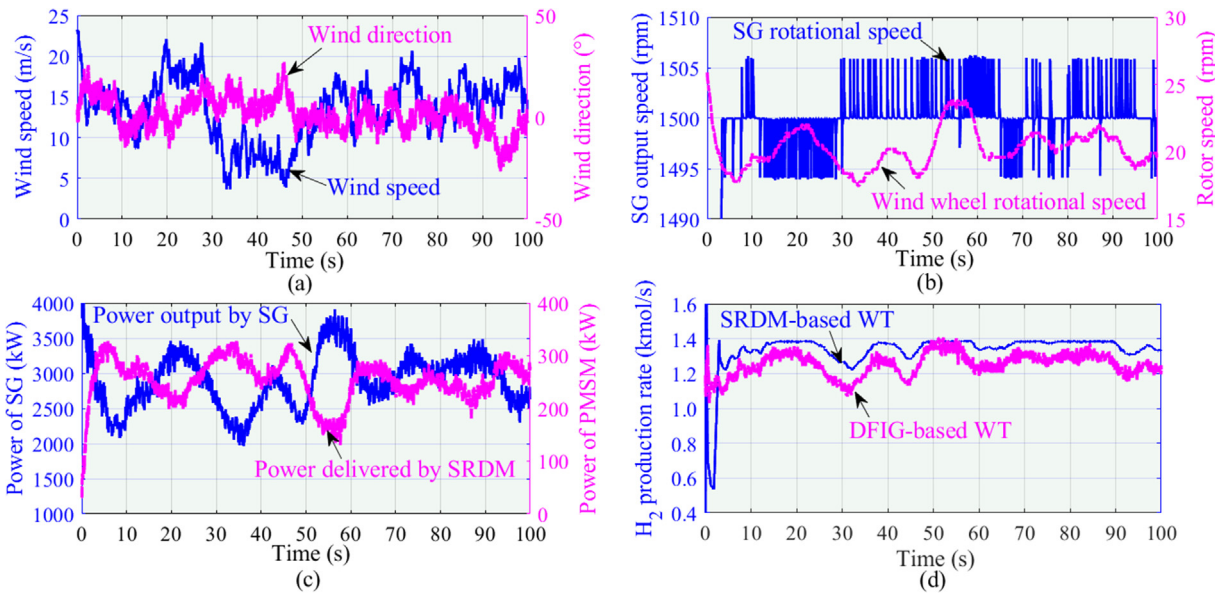


FIG. 9. Operating performance results of the proposed system under case (2): (a) wind wheel input, (b) speeds of wind wheel and SG, (c) power delivered by SG and SRDM, and (d) hydrogen production rates with SRDM- and DFIG-based WTs.

The maximum steady-state fluctuation at a particular load is within 11.51%, while the maximum difference of the power output by SRDM-based WT reaches 23.67%.

C. Operating performance under fault conditions

In order to ascertain the improved LVRT capability, the on-grid performances of DFIG-based WT, SRDM-based WT, and the proposed

SRDM-based WT with HSS are compared in the presence of different grid faults. Namely, case (5): a three-phase voltage symmetrical fault with a dropping depth of 0.80 p.u. for 500 ms and case (6): a voltage asymmetrical line-to-line fault with a dropping depth of 0.80 p.u. for 150 ms. Comparative results of generator key indicators, including stator currents, electromagnetic torques, and reactive powers under case (5) and case (6), are collected in Figs. 13 and 14, respectively.

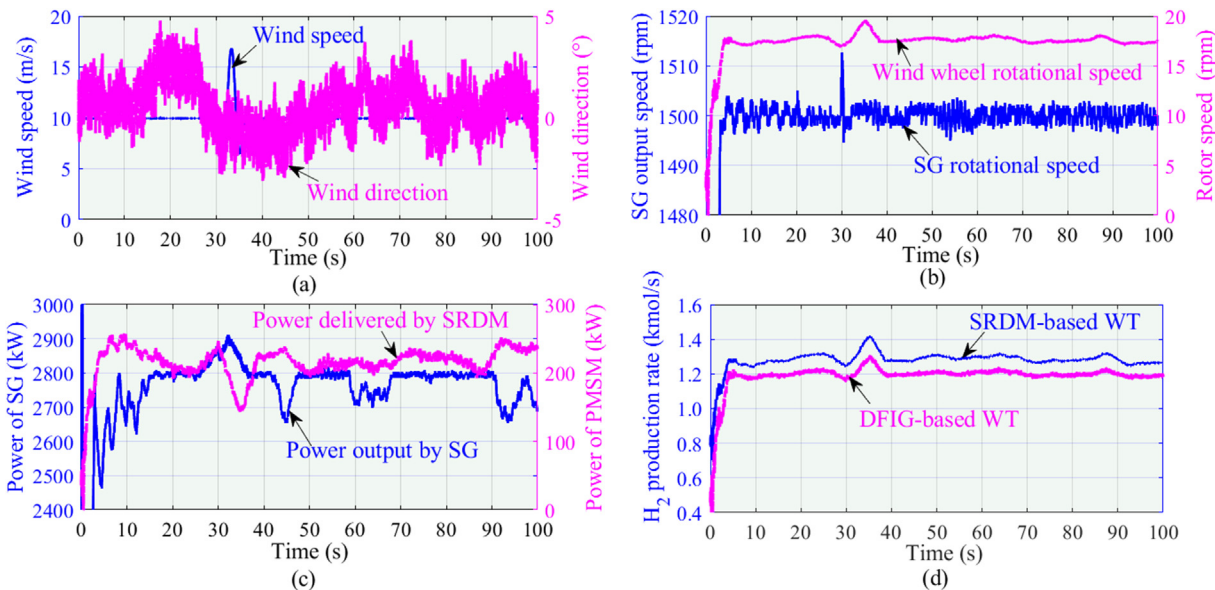


FIG. 10. Operating performance results of the proposed system under case (3): (a) wind wheel input, (b) speeds of wind wheel and SG, (c) power delivered by SG and SRDM, and (d) hydrogen production rates with SRDM- and DFIG-based WTs.

20 May 2024 01:52:06

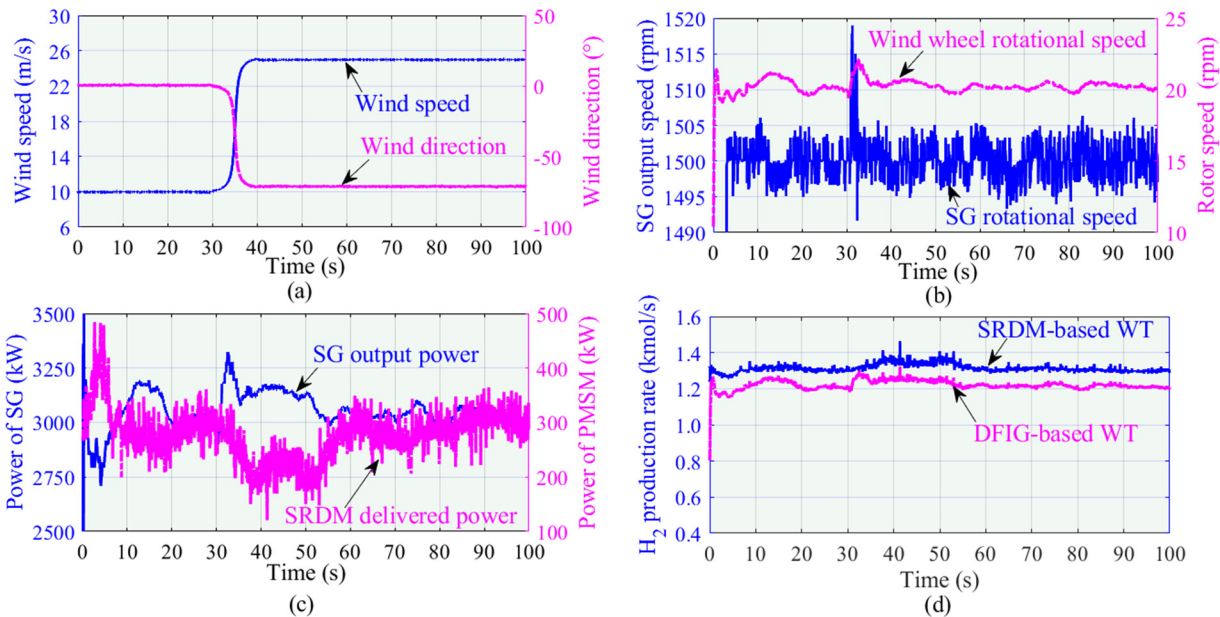


FIG. 11. Operating performance results of the proposed system under case (4): (a) wind wheel input, (b) speeds of wind wheel and SG, (c) power delivered by SG and SRDM, and (d) hydrogen production rates with SRDM- and DFIG-based WTs.

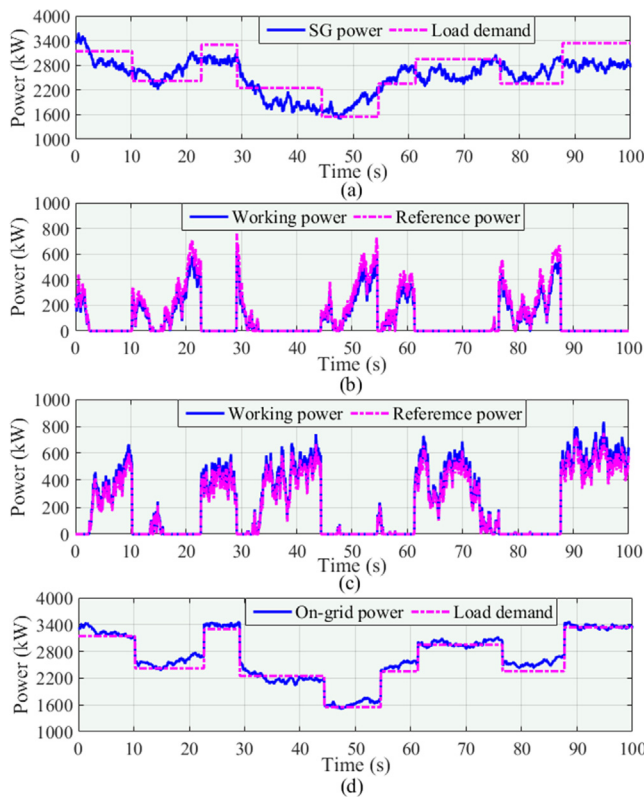


FIG. 12. Power balance results of SRDM-based WT with HSS: (a) SG generated power and load demand, (b) power consumed by the electrolyzer, (c) power provided by PEMFC, and (d) on-grid power and load demand.

When the fault case (5) happens, it is self-evident from Fig. 13 that the transient stator current and electromagnetic torque of SRDM-based WT with HSS have smaller oscillation peak or bottom with the levels of 1.98 and 0.31 p.u., respectively, which account for only about 85% and 55% of those for SRDM-based WT without HSS and DFIG-based WT. The shortest times are required for the indicators of the proposed system to return to the steady states after the fault period. Moreover, as seen in Fig. 13(c), both the SRDM-based WTs with/without HSS are able to provide over 0.5 p.u. reactive power to the grid, such that the reactive power support capacity can be guaranteed. When the asymmetrical line-to-line fault occurs, the recorded parameters vibrate more severely, especially for the DFIG-based WT. However, the SRDM-based WT with HSS still shows satisfactory LVRT capability. Comparative results well-verify the practicality and superiority of the developed wind-hydrogen power generation system.

It is worth mentioning that the SRDM-based WT also shows fairly good on-grid performance during LVRT periods owing to the satisfactory ability for SG excitation to compensate for the negative sequence component and provide reactive power to support the grid voltage restoration. However, by integrating HSS to SRDM-based WT, the grid-connected performance of the wind-hydrogen system can be further promoted since HSS is able to consume the residual instantaneous power during grid-voltage faults. Moreover, HSS is also helpful for relieving the on-grid power fluctuations of SRDM-based WT, by which the system's continuous operating stability can be improved.

## VI. CONCLUSIONS

Aiming at the proposed wind-hydrogen power generation unit, this paper investigates the advanced energy management and capacity allocation strategies to realize the stable, economical, and friendly operation of SRDM-based WT with HSS, under the uncertainties from the wind power output and load demand. PSO solves the optimal

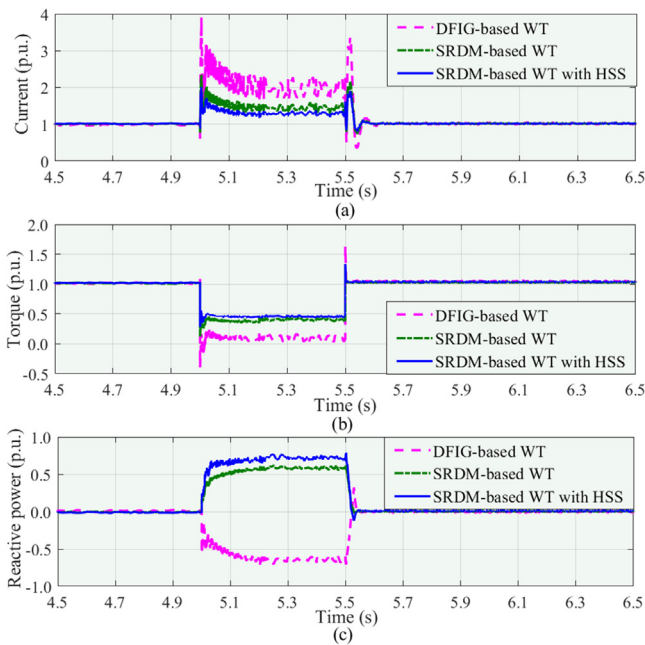


**FIG. 13.** Comparative results of the on-grid performance under case (5): (a) magnitude of stator current, (b) SG electromagnetic torque, and (c) reactive power to the grid.

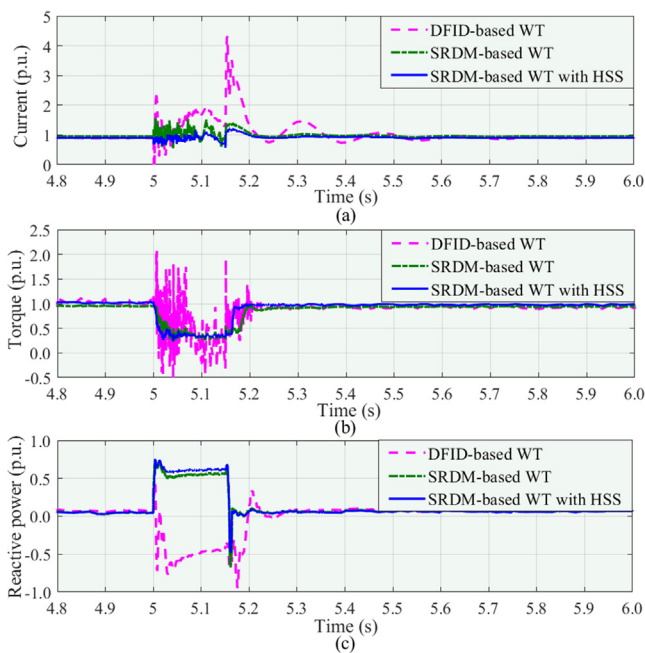


**FIG. 14.** Comparative results of the on-grid performance under case (6): (a) magnitude of stator current, (b) SG electromagnetic torque, and (c) reactive power to the grid.

sizing model with different wind power utilization levels. The influences of the investment cost and working efficiency on capacity allocation results are analyzed. PSO solutions indicate that, the promotion of wind power utilization level means the expansion of the capacity of HSS, but the decrease in project benefits. Finally, a series of experimental and simulation studies are carried out to verify the operational feasibility and superiority of the proposed scheme.

The results show that (i) SRDM, working as a speed regulator, can efficiently make SG produce constant frequency power under different wind conditions. (ii) The power dissipation of PMSM is relatively small and accounts for only 17.73% for a 3 MW WT. Compared to the existing DFIG-based WT, SRDM-based WT possesses higher transmission efficiency and can produce about 5.84%–7.51% more hydrogen in the same working situations. (iii) Under normal conditions, HSS can not only quickly compensate for the gap between SG output power and load demand but also drastically alleviate the instant fluctuations of system on-grid power. (iv) During the voltage drop periods, SRDM-based WT with HSS has outstanding LVRT capability. Moreover, the SG stator current oscillation peaks are less than 1.98 p.u., while the oscillation bottoms of electromagnetic torque are bigger than 0.31 p.u. The proposed system is also able to provide sufficient reactive power for the grid restoration to the normal operating state.

The results of this paper may provide significant technical references for improving the operation stability, flexibility, and economy of the developing new-type power systems with high renewable penetrations. In future studies, validation works in a high-power experimental platform can be conducted to improve the proposed wind–hydrogen energy system as well as the designed energy management and optimal allocation strategies.

## ACKNOWLEDGMENTS

The research presented in this paper was supported by the Open Fund of Key Laboratory of Modern Power Simulation and Control & Renewable Energy Technology, Ministry of Education (Northeast Electric Power University) under Grant No. MPSS2022–02, the National Natural Science Foundation of China under Grant No. 52005306, and the Shandong Provincial Natural Science Foundation under Grant No. ZR2020QE220. The authors acknowledge Professor Youguang Guo and Dr. Gang Lei from University of Technology Sydney, Australia for discussions regarding the optimization model and solving algorithm.

## AUTHOR DECLARATIONS

### Conflict of Interest

The authors have no conflicts to disclose.

### Author Contributions

**Wenliang Yin:** Conceptualization (equal); Data curation (equal); Formal analysis (equal); Funding acquisition (equal); Investigation (equal); Methodology (equal); Project administration (equal); Resources (equal); Software (equal); Supervision (equal); Validation (equal); Visualization (equal); Writing – original draft (equal); Writing – review & editing (equal). **Lin Liu:** Conceptualization (equal); Data curation (equal); Formal analysis (equal); Methodology (equal); Supervision (equal);

Writing – review & editing (equal). **Yue Wang:** Formal analysis (equal); Investigation (equal); Software (equal); Writing – original draft (equal); Writing – review & editing (equal). **Ziwei Wang:** Conceptualization (equal); Investigation (equal); Methodology (equal); Software (equal); Validation (equal); Writing – original draft (equal). **Junhui Li:** Conceptualization (equal); Funding acquisition (equal); Project administration (equal); Supervision (equal); Writing – review & editing (equal).

**DATA AVAILABILITY**

The data that support the findings of this study are available from the corresponding author upon reasonable request.

**APPENDIX A: PARAMETERS AND DATA**

All the electrolyzer parameters are listed in Table I. According to the analysis of the relationships between each parameter and their effects on the optimization results, the key parameters for solving the optimization model are given in Table II. Specifically, due to the needs from the optimization model, the WT output powers at different periods are collected in Table II. The average investment, operation and maintenance costs, service time span, as well as the operating efficiency of each system equipment are also recorded in Table II. Additionally, the prices

**TABLE I.** The parameters of the electrolyzer.

Parameters	Values	Parameters	Values
$a_1$ ( $\Omega \text{ m}^2$ )	$7.33 \times 10^{-5}$	$d_1$ (%)	99.50
$a_2$ ( $\Omega \text{ m}^2 \text{ }^\circ\text{C}^{-1}$ )	$-1.11 \times 10^{-7}$	$d_2$ ( $\text{m}^2 \text{ A}^{-1}$ )	-9.58
$b_1$ (V)	0.16	$d_3$ ( $\text{m}^2 \text{ A}^{-1} \text{ }^\circ\text{C}^{-1}$ )	$-5.55 \times 10^{-2}$
$b_2$ ( $\text{V }^\circ\text{C}^{-1}$ )	$1.38 \times 10^{-3}$	$d_4$ ( $\text{m}^2 \text{ A}^{-1} \text{ }^\circ\text{C}^{-2}$ )	0
$b_3$ ( $\text{V }^\circ\text{C}^{-2}$ )	$-1.61 \times 10^{-5}$	$d_5$ ( $\text{m}^4 \text{ A}^{-1}$ )	$1.50 \times 10^3$
$c_1$ ( $\text{m}^2 \text{ A}^{-1}$ )	$-1.60 \times 10^{-2}$	$d_6$ ( $\text{m}^4 \text{ A}^{-1} \text{ }^\circ\text{C}^{-1}$ )	-70.80
$c_2$ ( $\text{m}^2 \text{ A}^{-1} \text{ }^\circ\text{C}$ )	-1.30	$d_7$ ( $\text{m}^4 \text{ A}^{-1} \text{ }^\circ\text{C}^{-2}$ )	0
$c_3$ ( $\text{m}^2 \text{ A}^{-1} \text{ }^\circ\text{C}^2$ )	4.12	$N_{el}$	500–1000
$A_{el}$ ( $\text{m}^2$ )	0.25	$T_{el}$ ( $^\circ\text{C}$ )	25

of on-grid wind power, on-grid PEMFC electricity, hydrogen, as well as the average benefit from environmental protection are given in Table II.

**APPENDIX B: ENERGY MANAGEMENT STRATEGY**

The principles of the eight-modes-based power supervision approach and the corresponding model selection process are depicted in Figs. 15 and 16, respectively. Coupled with the

**TABLE II.** Key parameters and data for capacity allocation solving: (a) output power data of SRDM-based WT in a day, (b) average cost and operating data of equipment, and (c) benefit data of products.

(a)					
Periods (h)	$P_{WT,t}$ (MW)	Periods (h)	$P_{WT,t}$ (MW)	Periods (h)	$P_{WT,t}$ (MW)
1	2.93	9	2.45	17	2.13
2	2.90	10	2.33	18	2.39
3	2.86	11	2.24	19	2.49
4	2.84	12	2.08	20	2.58
5	2.77	13	1.94	21	2.70
6	2.73	14	1.81	22	2.78
7	2.69	15	1.88	23	2.87
8	2.51	16	1.96	24	2.96
(b)					
Equipment	Investment cost (Yuan/kW)	Operating cost (%)	Service time (year)	Efficiency (%)	
WT	6500	5	20	None	
Electrolyzer	5800	5	20	76	
PEMFC	4800	5	20	58	
Compressor	850	1	20	90	
Storage tank	55	1	20	95	
Supercapacitor	2200	5	20	95	
(c)					
Items	WT (Yuan/kWh)	PEMFC (Yuan/kWh)	Hydrogen (Yuan/kg)	Environment (Yuan/kWh)	
Prices	0.44	0.52	31.50	0.038	

20 May 2024 01:52:06

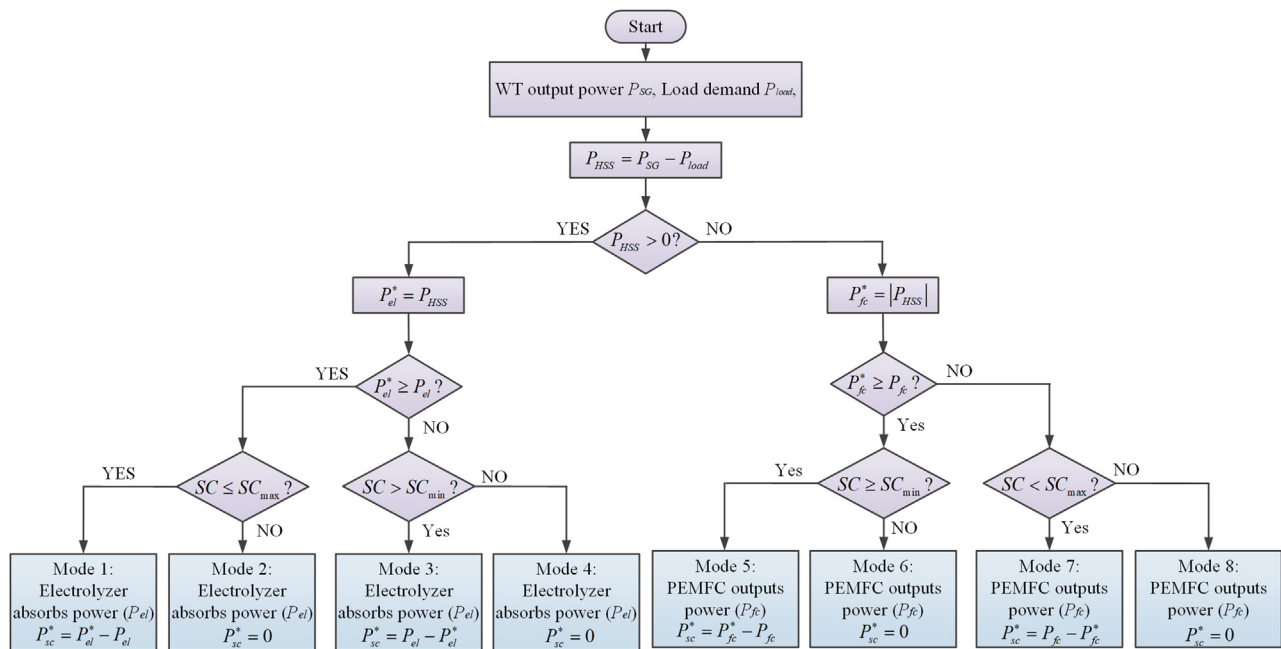


FIG. 15. Process principles of the eight-modes-based energy management strategy.

equipment-level controllers, the autonomous and stable operation of the proposed wind–hydrogen system, with the required energy measurements, decisions, and controls, can be realized.

In Figs. 15 and 16,  $P_{el}^*$ ,  $P_{fc}^*$ , and  $P_{sc}^*$  are the reference powers of electrolyzer, PEMFC, and supercapacitor.  $SC$  is the state of charge for supercapacitor, while  $SC_{min}$  and  $SC_{max}$  are the minimum and maximum of  $SC$ . As shown, eight operating modes are distinguished based on different working states of HSS, as follows.

- (i)  $P_{el}^* \geq P_{el}$  and  $SC \leq SC_{max}$ . The electrolyzer absorbs power ( $P_{el}$ ), while the supercapacitor consumes power ( $P_{sc}^* = P_{el}^* - P_{el}$ ) to alleviate the power imbalance caused by the electrolyzer slow dynamic response.
- (ii)  $P_{el}^* \geq P_{el}$  and  $SC > SC_{max}$ . The electrolyzer absorbs power ( $P_{el}$ ), while the supercapacitor stops working due to the saturated charging state.
- (iii)  $P_{el}^* < P_{el}$  and  $SC > SC_{min}$ . The electrolyzer absorbs power ( $P_{el}$ ), while the supercapacitor provides power ( $P_{sc}^* = P_{el} - P_{el}^*$ ).
- (iv)  $P_{el}^* < P_{el}$  and  $SC \leq SC_{min}$ . The electrolyzer absorbs power ( $P_{el}$ ), while the supercapacitor stops working due to the empty charging state.
- (v)  $P_{fc}^* \geq P_{fc}$  and  $SC \geq SC_{min}$ . PEMFC outputs power ( $P_{fc}$ ), and the supercapacitor also outputs power ( $P_{sc}^* = P_{fc}^* - P_{fc}$ ).
- (vi)  $P_{fc}^* \geq P_{fc}$  and  $SC < SC_{min}$ . PEMFC outputs power ( $P_{fc}$ ), and the supercapacitor stops working.
- (vii)  $P_{fc}^* < P_{fc}$  and  $SC < SC_{max}$ . PEMFC outputs power ( $P_{fc}$ ), and the supercapacitor absorbs difference power ( $P_{sc}^* = P_{fc} - P_{fc}^*$ ).

- (viii)  $P_{fc}^* < P_{fc}$  and  $SC \geq SC_{max}$ . PEMFC outputs power ( $P_{fc}$ ), and the supercapacitor stops working.

### APPENDIX C: CONTROL STRATEGIES OF SRDM-BASED WT

As describe above, the adaptive neuro-fuzzy pitch angle control method, referenced by Petković's work,<sup>20</sup> was used for the pitch angle control. Considering the parameter uncertainties and disturbances in the grid, such as sudden load fluctuation and sub-synchronous resonance, an adaptive robust backstepping control strategy, equipped with an extended state observer, was synthesized for the high precision speed tracking of SRDM. The control law was designed as<sup>19</sup>

$$\begin{cases} u = (u_a + u_s)/\hat{\theta}_1, \\ u_a = \dot{x}_{1d} + \hat{\theta}_2 x_1 - \hat{x}_2, \\ u_s = u_{s1} + u_{s2}, \\ u_{s1} = -k_1 z_1, \end{cases} \quad (C1)$$

where  $x_1 = \omega_m$  is the angular velocity of PMSM,  $x_{1d}$  is the desired value of  $x_1$ ,  $z_1 = x_1 - x_{1d}$  is the switching function.  $\theta = [\theta_1 \ \theta_2]^T = [k_t/J \ B/J]^T$ , in which  $J$ ,  $B$ , and  $k_t$  are the rotational inertia, viscous friction coefficient, and torque coefficient of PMSM.  $u_a$  is the adjustable model compensation to achieve perfect tracking, and  $u_s$  is the robust control law consisting of  $u_{s1}$  and  $u_{s2}$ .  $u_{s1}$  is the proportional feedback to stabilize the nominal system, while  $u_{s2}$  represents the robust control function which can be used to attenuate the effects of model uncertainties.

The control system structure diagram is presented in Fig. 17.

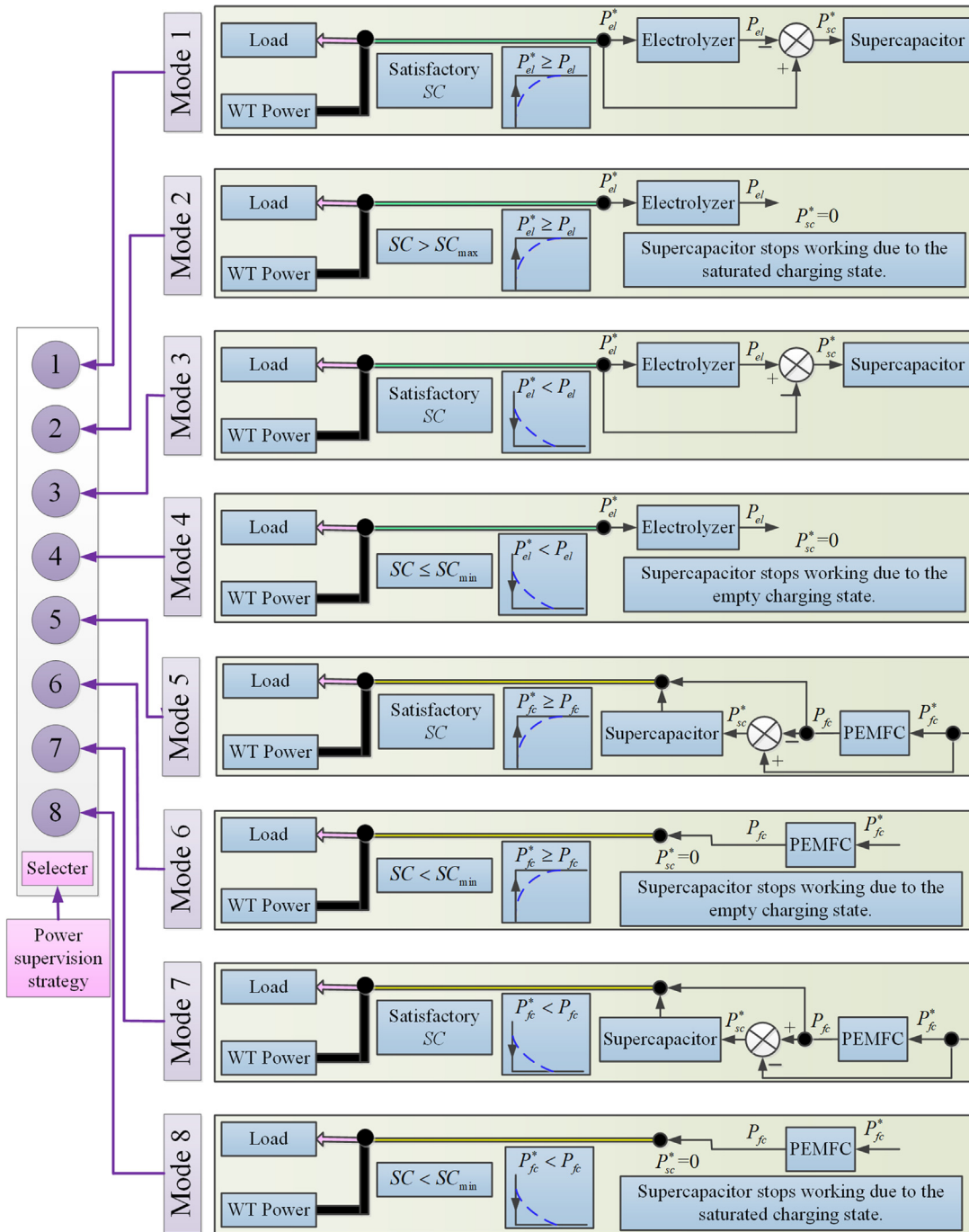


FIG. 16. Mode selection process of the energy management strategy.

After completing the SRDM speed adjustment, combined with the backstepping design method and the sliding mode control theory, an advanced backstepping sliding mode excitation control approach with an extended state observer (ESO) was proposed to realize the

dynamic compensation of nonlinear factors and uncertain disturbances in SG operation and terminal voltage tracking.<sup>38</sup> Two design processes are required for the excitation control method, i.e., design of the ESO and design of the backstepping sliding mode control law.



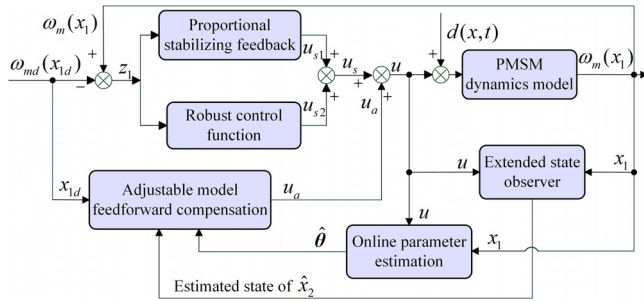


FIG. 17. Structure diagram of PMSM speed control method.<sup>19</sup>

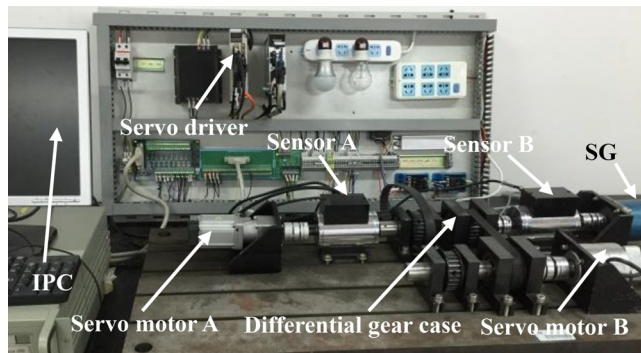


FIG. 18. Experimental construction of SRDM-based WT.

A two-orders ESO was constructed to observe external disturbances in real time, given as follows:<sup>38</sup>

$$\begin{cases} e = m_1 - x_3, \\ \dot{m}_1 = m_2 - \beta_1 \text{fal}(e, \gamma_1, \zeta) + \frac{x_2 x_3}{H} \cot \frac{x_1}{H} + b_0 u, \\ \dot{m}_2 = -\beta_2 \text{fal}(e, \gamma_2, \zeta), \end{cases} \quad (C2)$$

where  $x_1 = H\delta$ ,  $x_2 = H(\omega - \omega_0)$ , and  $x_3 = -\omega_0 P_e$ .  $\delta$ ,  $P_e$ , and  $\omega$  are the power angle, electromagnetic power, and rotor speed.  $\omega_0$  is the initial rotor speed, and  $H$  is the inertial time constant.  $m_1$  and

$m_2$  are the estimated values of  $x_3$  and disturbance.  $\beta_1$  and  $\beta_2$  are the bandwidth parameters of the observer.  $\gamma_1$  and  $\gamma_2$  are the index change parameters of observation error, and  $\zeta$  is the length of the linear interval of the observer, which are a set of fixed constant values located in  $(0, 1)$ .  $\text{fal}$  is a nonlinear function and<sup>38</sup>

$$\text{fal}(e, \gamma, \zeta) = \begin{cases} \frac{e}{\zeta^{\gamma-1}}, & |e| \leq \zeta, \\ |e|^\gamma \text{sign}(e), & |e| > \zeta. \end{cases} \quad (C3)$$

In accordance with the principle of backstepping sliding mode control, aiming at the three-order SG model, the final control law was designed as<sup>38</sup>

$$u = \frac{1}{b_0} \left[ -k\dot{z}_2 - m_2 - \frac{1}{H} x_2 x_3 \cot \frac{x_1}{H} + \dot{\alpha}_2 - \varepsilon_1 (s + \varepsilon_2 \text{sat } s) \right], \quad (C4)$$

where  $b_0$  is an intermediate variable related to the SG characteristics.  $z_2 = x_2 - \alpha_1$  is a defined virtual state variable.  $\alpha_1$  and  $\alpha_2$  are the virtual control quantities to make the respective subsystems stable.  $\varepsilon_1$ ,  $\varepsilon_2$ , and  $k$  are all constants in the sliding surface function.  $\text{sat}$  is a saturation function.<sup>38</sup>

#### APPENDIX D: INTRODUCTION OF THE EXPERIMENTAL PLATFORM

Figure 18 shows the setup of the built experimental platform of SRDM-based WT. The block diagram of operating principles of the testbed is described in Fig. 19. Differential gear box, treated as the core equipment of the testbed, consists of a single-stage planetary gear and a pair of synchronous belt wheels.

Servo motors “A” and “B,” connected to the planet carrier and ring gear of differential gear box, are, respectively, utilized to provide dominating input and speed regulation power source. Sensors A and B are employed to collect the real-time data of torque and speed signals that will be transferred to the industrial personal computer (IPC) to finish the speed control process. DAQNav, MATLAB, and LabVIEW are adopted to realize the connections between software and hardware equipment.

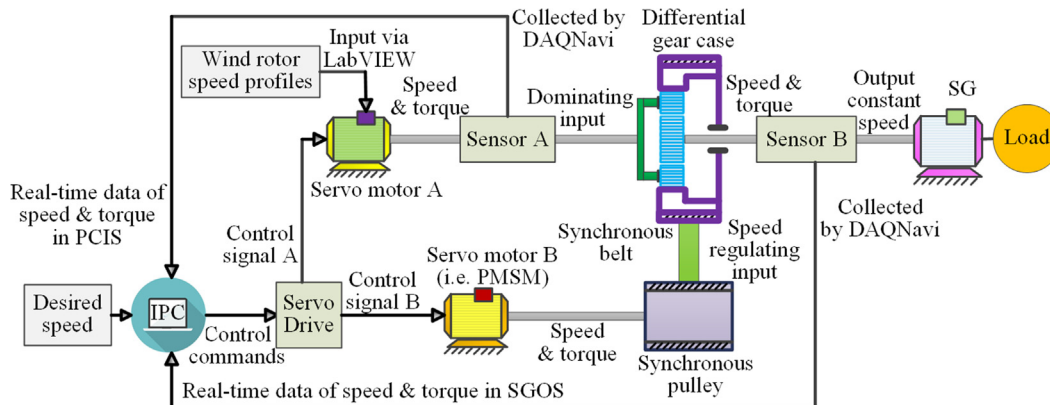


FIG. 19. Operating principles of the built experimental platform.

## REFERENCES

- <sup>1</sup>S. J. Zhang, W. Jing, X. Chen *et al.*, “China in global wind power development: Role, status and impact,” *Renewable Sustainable Energy Rev.* **127**, 109881 (2020).
- <sup>2</sup>Global Wind Energy Council, *Global Wind Report 2018* (Global Wind Energy Council, Istanbul, Turkey, 2019).
- <sup>3</sup>M. Zhang, J. Chen, Z. Yang *et al.*, “Stochastic day-ahead scheduling of irrigation system integrated agricultural microgrid with pumped storage and uncertain wind power,” *Energy* **237**, 121638 (2020).
- <sup>4</sup>F. Luo, K. Meng, Z. Y. Dong *et al.*, “Coordinated operational planning for wind farm with battery energy storage system,” *IEEE Trans. Sustainable Energy* **6**(1), 253–262 (2015).
- <sup>5</sup>H. Xu, J. Hu, and Y. He, “Operation of wind-turbine-driven DFIG systems under distorted grid voltage conditions: Analysis and experimental validations,” *IEEE Trans. Power Electron.* **27**(5), 2354–2366 (2012).
- <sup>6</sup>J. Carroll, A. McDonald, and D. McMillan, “Reliability comparison of wind turbines with DFIG and PMG drive trains,” *IEEE Trans. Energy Convers.* **30**(2), 663–670 (2015).
- <sup>7</sup>R. Liu, J. Yao, X. Wang *et al.*, “Dynamic stability analysis and improved LVRT schemes of DFIG-based wind turbines during a symmetrical fault in a weak grid,” *IEEE Trans. Power Electron.* **35**(1), 303–318 (2020).
- <sup>8</sup>T. Sajjad and M. Behnam, “A comprehensive review of low voltage ride through of doubly fed induction wind generators,” *Renewable Sustainable Energy Rev.* **57**, 412–419 (2016).
- <sup>9</sup>S. T. Tentzerakis and S. A. Papathanassiou, “An investigation of the harmonic emissions of wind turbines,” *IEEE Trans. Energy Convers.* **22**(1), 150–158 (2007).
- <sup>10</sup>M. Kesraoui, A. Chaib, A. Meziane *et al.*, “Using a DFIG based wind turbine for grid current harmonics filtering,” *Energy Convers. Manage.* **78**, 968–975 (2014).
- <sup>11</sup>V. Yaramasu, B. Wu, S. Alepuz *et al.*, “Predictive control for low-voltage ride-through enhancement of three-level-boost and NPC-converter-based PMSG wind turbine,” *IEEE Trans. Ind. Electron.* **61**(12), 6832–6843 (2014).
- <sup>12</sup>M. Idan and D. Lior, “Continuously variable speed wind turbine transmission concept and robust control,” *Wind Eng.* **24**(3), 151–167 (2000).
- <sup>13</sup>Y. G. Lin, L. Tu, H. W. Liu *et al.*, “Hybrid power transmission technology in a wind turbine generation system,” *IEEE/ASME Trans. Mechatron.* **20**(3), 1218–1225 (2015).
- <sup>14</sup>D. Jelaska, S. Podrug, and M. Perkušić, “A novel hybrid transmission for variable speed wind turbines,” *Renewable Energy* **83**, 78–84 (2015).
- <sup>15</sup>W. L. Yin, Z. Y. Dong, L. Liu *et al.*, “Self-stabilising speed regulating differential mechanism for continuously variable speed wind power generation system,” *IET Renewable Power Gen.* **14**(15), 3002–3009 (2020).
- <sup>16</sup>X. Yin, Y. Li, and W. Li, “Operating modes and control strategy for megawatt-scale hydro-viscous transmission-based continuously variable speed wind turbines,” *IEEE Trans. Sustainable Energy* **6**(4), 1553–1564 (2015).
- <sup>17</sup>Q. Liu, R. Appunn, and K. Hameyer, “Wind turbine with mechanical power split transmission to reduce the power electronic devices: An experimental validation,” *IEEE Trans. Ind. Electron.* **64**(11), 8811–8820 (2017).
- <sup>18</sup>X. M. Rui, W. L. Yin, Y. X. Dong *et al.*, “Fractional-order sliding mode control for hybrid drive wind power generation system with disturbances in the grid,” *Wind Energy* **22**(1), 49–64 (2019).
- <sup>19</sup>W. L. Yin, X. Wu, X. M. Rui *et al.*, “Adaptive robust backstepping control of the speed regulating differential mechanism for wind turbines,” *IEEE Trans. Sustainable Energy* **10**(3), 1311–1318 (2019).
- <sup>20</sup>D. Petković, Ž. Cojbašić, V. Nikolić *et al.*, “Adaptive neuro-fuzzy maximal power extraction of wind turbine with continuously variable transmission,” *Energy* **64**, 868–874 (2014).
- <sup>21</sup>D. Y. Li, W. C. Cai, P. Li *et al.*, “Dynamics and control for a novel front-end speed regulation (FESR) wind turbine,” *IEEE Trans. Power Electron.* **33**(5), 4073–4087 (2018).
- <sup>22</sup>X. Li, H. Dong, H. Li *et al.*, “Optimization control of front-end speed regulation (FESR) wind turbine based on improved NSGA-II,” *IEEE Access* **7**, 45583–45593 (2019).
- <sup>23</sup>X. Yin, Y. Lin, W. Li *et al.*, “Hydro-viscous transmission based maximum power extraction control for continuously variable speed wind turbine with enhanced efficiency,” *Renewable Energy* **87**, 646–655 (2016).
- <sup>24</sup>W. L. Yin, X. M. Rui, L. Liu *et al.*, “Operating performance analysis on wind turbines with the speed regulating differential mechanism,” *J. Renewable Sustainable Energy* **10**(6), 063301 (2018).
- <sup>25</sup>X. Luo, J. Wang, M. Dooner *et al.*, “Overview of current development in electrical energy storage technologies and the application potential in power system operation,” *Appl. Energy* **137**, 511–536 (2015).
- <sup>26</sup>A. G. Olabi, C. Onumaegbub, T. Wilberforce *et al.*, “Critical review of energy storage systems,” *Energy* **214**, 118987 (2021).
- <sup>27</sup>H. Li, X. Yao, M. A. Tachea *et al.*, “Path selection for wind power in China: Hydrogen production or underground pumped hydro energy storage,” *J. Renewable Sustainable Energy* **13**, 035901 (2021).
- <sup>28</sup>K. E. Okedu, “Hydrogen production using variable and fixed speed wind farm topologies in a utility grid,” *J. Renewable Sustainable Energy* **8**, 063307 (2016).
- <sup>29</sup>T. Yuan, X. Dong, X. Chen *et al.*, “Energetic macroscopic representation control method for a hybrid-source energy system including wind, hydrogen, and fuel cell,” *J. Renewable Sustainable Energy* **10**, 043308 (2018).
- <sup>30</sup>W. Zhang, A. Maleki, F. Pourfayaz *et al.*, “An artificial intelligence approach to optimization of an off-grid hybrid wind/hydrogen system,” *Int. J. Hydrogen Energy* **46**(24), 12725–12738 (2021).
- <sup>31</sup>M. J. Khan and M. T. Iqbal, “Analysis of a small wind-hydrogen stand-alone hybrid energy system,” *Appl. Energy* **86**(11), 2429–2442 (2009).
- <sup>32</sup>A. Abdelkafi and L. Krichen, “Energy management optimization of a hybrid power production unit based renewable energies,” *Int. J. Electr. Power Energy Syst.* **62**, 1–9 (2014).
- <sup>33</sup>W. Yin, L. Liu, X. Rui *et al.*, “Analysis, modeling and control of a hybrid drive wind turbine with hydrogen energy storage system,” *IEEE Access* **8**, 114795–114806 (2020).
- <sup>34</sup>W. L. Yin, L. Liu, C. S. Zhang *et al.*, “Modeling and operation performance analysis of hybrid drive wind power generation system with hydrogen energy storage,” *Electr. Power Autom. Equip.* **40**(10), 64–70 (2020).
- <sup>35</sup>M. Y. Luo, *Planetary Gear Mechanism* (Higher Education Press, Beijing, China, 1984), pp. 13–21.
- <sup>36</sup>A. Bouscayrol, P. Delarue, and X. Guillaud, “Power strategies for maximum control structure of a wind energy conversion system with a synchronous machine,” *Renewable Energy* **30**(15), 2273–2288 (2005).
- <sup>37</sup>Y. Zhang, Z. Y. Dong, F. J. Luo *et al.*, “Optimal allocation of battery energy storage systems in distribution networks with high wind power penetration,” *IET Renewable Power Gen.* **10**(8), 1105–1113 (2016).
- <sup>38</sup>Z. Wang, W. Yin, L. Liu *et al.*, “Grid-connected control of hybrid drive wind turbine based on backstepping sliding mode,” *Electr. Power Autom. Equip.* **43**(3), 117–123 (2023).
- <sup>39</sup>H. Zhao, B. Wang, X. Wang *et al.*, “Active Dynamic aggregation model for distributed integrated energy system as virtual power plant,” *J. Mod. Power Syst. Clean Energy* **8**(5), 831–840 (2020).
- <sup>40</sup>Standardization Administration of China, “Power quality-frequency deviation for power system,” Chinese Standard No. GB/T15945-2008, 2009.